Nuclear Inst. and Methods in Physics Research, A 987 (2021) 164840

Contents lists available at ScienceDirect

Nuclear Inst. and Methods in Physics Research, A

journal homepage: www.elsevier.com/locate/nima

Novel strategies for fine-segmented Low Gain Avalanche Diodes

G. Paternoster [a,b,*], G. Borghi [a,b], R. Arcidiacono [c,f], M. Boscardin [a,b], N. Cartiglia [c], M. Centis Vignali [a], G.F. Dalla Betta [d,b], M. Ferrero [f], F. Ficorella [a,b], M. Mandurrino [c], L. Pancheri [d,b], F. Siviero [c,e], V. Sola [c,e], M. Tornago [c,e]

[a] Fondazione Bruno Kessler, Centre of Materials and Microsystems, Trento, Italy
[b] TIFPA-INFN, via Sommarive 18, 38123, Trento, Italy
[c] INFN, Torino, Italy
[d] Università di Trento, Trento, Italy
[e] Università di Torino, Torino, Italy
[f] Università del Piemonte Orientale, Italy

ARTICLE INFO

MSC:
00-01
99-00

Keywords:
Silicon sensors
Fast detectors
LGAD
TI-LGAD
RSD
AC-LGAD
4D-tracking

ABSTRACT

Low Gain Avalanche Diodes (LGADs) are now considered a viable solution for 4D-tracking thanks to their excellent time resolution and good resistance to high radiation fluence. However, the currently available LGAD technology is well suited only for applications that require coarse space precision, pixels with pitch in the range 500 μm–1 mm, due to the presence of a no-gain region between adjacent pixels of about 50 μm, in which the gain is completely suppressed. In this paper, we will discuss the segmentation issues in the LGAD technology and we will present two new segmentation strategies aimed at producing LGADs with high spatial resolution and high fill factor. The first presented design is the so-called Trench-Isolated LGAD (TI-LGAD). Here, the pixel isolation is provided by trenches, physically etched in the silicon and then filled with silicon oxide. The second design is the Resistive AC-coupled Silicon Detector (RSD), an evolution of LGADs, where the segmentation is obtained by means of AC-coupled electrodes.

Prototypes of both designs have been produced at FBK and characterized at the Laboratories for Innovative Silicon Sensors (INFN and University of Turin) by means of a laser setup to estimate the space resolution and the fill factor. The functional characterization shows that both the technologies yield fully working small pixel LGADs (down to 50 μm), providing the first examples of sensors able to concurrently measure space and time with excellent precision.

1. Introduction

Low Gain Avalanche Diodes (LGADs) are silicon sensors based on p–n junction and provided with an internal signal amplification mechanism (gain) [1]. The internal structure is similar to that of silicon Avalanche Photodiodes (APDs), but the gain is much lower ($\mathcal{O}(10)$ with respect to $\mathcal{O}(1000)$ of APD). The combination of low gain and thin active silicon substrates already made LGADs a viable choice for those applications that requires good time resolution and high resistance to radiation, as in the case of detectors for High Energy Physics (HEP) experiments [2,3].

Another important feature of LGADs is the possibility to arrange the single diodes in large-area segmented sensors (pixel arrays or strips), which are able to provide information on both time and position of interaction of the detected particles.

The latter aspect is a key enabling feature for the so-called "4-dimensional (4D) tracking", which requires a concurrently $\mathcal{O}(10)$ ps time resolution and a $\mathcal{O}(10)$ μm space resolution in Minimum Ionizing Particles (MIP) detection [4]. A first example of a LGAD designed for 4D tracking are the Ultra Fast Silicon Detectors (UFSDs), which have been developed for the High Luminosity (HL) upgrade of LHC. These sensors reach the required specifications in terms of radiation hardness, space and time resolution [5–7]. However, additional development has to be done to meet the requests of the next generation of HEP experiments and those of other applications, such as x-ray imaging or ion tracking in devices for medical applications (hadrontherapy) [8,9].

The current R&D activities on LGADs are focused on three different goals, interconnected with each other: (i) improvement of the time resolution; (ii) increase of the radiation hardness beyond 10^{15} neq/cm^2 (where neq stands for 1-MeV-neutron-equivalent damage); (iii) improvement of the spatial resolution. This paper is focused on the latter task, which has been also the least investigated by the scientific community in the past few years.

* Corresponding author at: Fondazione Bruno Kessler, Centre of Materials and Microsystems, Trento, Italy.
E-mail address: paternoster@fbk.eu (G. Paternoster).

https://doi.org/10.1016/j.nima.2020.164840
Received 31 March 2020; Received in revised form 29 October 2020; Accepted 3 November 2020
Available online 5 November 2020
0168-9002/

In the following section, we discuss the current state-of-the-art technology for segmenting LGADs, pointing out its limiting factors. In Section 3 we introduce two new segmentation strategies to develop fine-pitch LGADs. The first proposed scheme is the so-called Trench-Isolated LGAD (TI-LGAD), while the second is the Resistive AC-coupled Silicon Detector (RSD). In both cases, experimental characterization will be shown and discussed.

2. Segmentation of standard LGAD

A schematic drawing of the internal structure of a n-in-p diode array (PIN) and of a segmented LGAD is shown in Fig. 1. PIN diode arrays are usually based on a segmented n^+ junction on a high-resistivity p-type substrate and the electrical isolation among pixels is usually provided by a p-doped region (p-stop) that surrounds each pixel.

Segmented silicon detectors with internal multiplication need to face additional hurdles with respect to conventional PIN arrays. The typical design of a segmented LGAD (also named "standard LGAD" later in the text) is represented in Fig. 1b. The basic multiplying structure is based on a shallow n^+ junction and on a deep p-type multiplication layer below the junction. This doped region, also named "gain layer", locally increases the electric field to values higher than the impact-ionization threshold (about $2 \times 10^5\,\mathrm{V\,cm^{-1}}$), enabling the mechanism responsible of charge multiplication. When segmented, beside the p-stop isolation region, these multiplying junctions require a complex design of the border region, in order to avoid undesired regions with high electric field [10]. Therefore, an additional n-type region, named Junction Termination Extension (JTE), is typically included at the n^+ periphery, with the role to control the junction curvature and reduce the electric field at the border. The gain layer is also interrupted below the JTE and at the p-stop regions, also in this case to reduce the electric field and prevent premature breakdown at the pixel edge (or edge-breakdown). To further control the edge electric field, the gain layer is also kept at a certain distance from the edge of the JTE, in order to create the so-called virtual guard ring (vGR).

As a consequence, a relatively wide gap is created between the gain layers of two adjacent pixels: this gap is called "no-gain" region, since the ionization produced by particles impinging in that area is not multiplied. This is represented in Fig. 1(c) and (d), where the signal produced by a particle as a function of the impinging position is represented for a PIN and an LGAD detector, respectively. In the case of a PIN diode, the charges generated by a particle interacting at the pixel periphery are typically shared among neighboring pixels and the sum of the signals from all the involved pixels is a constant. In the LGAD case, instead, the signal is multiplied only in the pixel core region and not at the pixel periphery, because the charges generated in this region are collected by the JTE and do not pass through the gain layer. As a consequence, the total signal is not constant but varies from a maximum value, corresponding to the nominal gain (G), to the minimum G = 1. We can define the fill factor (FF) of the LGAD pixel as

$$FF = \frac{\text{pixel area with signal multiplication}}{\text{total pixel area}}. \quad (1)$$

The minimum achievable width of the no-gain region depends on both technological and physical limitations since (i) the technological constraints of the fabrication process put a limit on the minimum achievable feature size and on the alignment precision which is achievable among different structures; (ii) a too small gap between n-doped regions and p-stop generates high electric fields that would lead to premature edge-breakdown and "pop-corn" noise [11].

In the past few years, several efforts have been made to reduce the width of the no-gain region, by optimizing both the fabrication technology and the sensor layout. Table 1 reports the evolution of the nominal no-gain width in the different batches produced at FBK in the last few years. In the first batch, the no-gain width was 210 μm and it has been reduced in the following productions down to 20.5 μm, a value that could be considered the state-of-the-art of the standard FBK-LGAD technology.

Table 1
Evolution of the no-gain width in FBK productions.

Batch	Year	No-gain width
UFSD 1 [7]	2016	210 μm
UFSD 2 [6,8]	2017	66 μm
UFSD 3 - Safe [12,13]	2018	31 μm
UFSD 3 - Intermediate [12,13]	2018	20.5 μm

An additional factor that could affect the FF of standard-LGADs is the uneven electric field at the pixel border, which could lead to spatial non-uniformity in the charge carriers collection and multiplication.

In order to understand this effect, TCAD simulations (Silvaco simulation tools [14]) have been exploited to investigate the collection mechanisms at the border region of the pixel. Fig. 2 represents the electric field (gray scale map) of a segmented LGAD (same structure represented in Fig. 1b), while the solid lines represent the carrier drift path lines, and the lines color is the ionization integral along that carrier path. The bias voltage is 200 V, and the gain at the pixel core is about 7. The ionization integral reaches a plateau (red lines, corresponding to the maximum gain) in the pixel core region, while it is almost zero in the no-gain region (purple lines). Moreover, it is possible to identify a third region, indicated as "transition region". In this region, the drift lines are bent by the curvature of the electric field and the carriers, even though generated in the nominal gain region, are only partially multiplied. The transition region reduces the effective FF of the pixel with respect to the nominal one. This effect becomes very important when the pixel size is small (< 100 μm) or in sensors with thick depleted region, because of the curvature of the carriers drift lines, as represented in Fig. 2. It is possible to define the "effective inter-pad width" as the distance between the two locations in adjacent pixels where the generated signals are equal to 50% of the maximum signal value, as represented in Fig. 1d. The width of the transition region could depend on multiple factors: (i) bias voltage, (ii) depletion-region thickness, (iii) lateral diffusion of the doped regions and (iv) doping concentration of the gain layer. An accurate simulation campaign of these effects is currently under way.

An experimental measurement of the signal variation at the pixel border of standard-LGAD is reported in Fig. 3. The measurement was performed at the Laboratories for Innovative Silicon Sensors of the INFN and University of Turin, using the Transient Current Technique (TCT) setup described in [12]. In this setup, a focused 1064 nm laser (spot size of ∼ 10 μm) is used to simulate the passage of a MIP in different position of the sensor pixel, directly measuring the sensor response in the inter-pad region.

The sensor in Fig. 3 is a standard-LGAD from FBK-UFSD3 batch production with a nominal no-gain region of 31 μm. It is worth noting that the measured inter-pad width is 38.0 ± 2.5 μm, wider than the nominal no-gain region. This is due to the presence of the transition region that increases the effective inter-pad width. A more quantitative discussion about the transition-region effect is reported in [15]

3. Novel segmentation schemes

In order to reduce the width of the no-gain region, novel detectors schemes have been recently proposed. Fig. 4 represents four different segmentation schemes:

(a) Standard LGAD;
(b) Double-sided LGAD (or inverted LGAD, i-LGAD);
(c) Trench-Isolated LGAD (TI-LGAD);
(d) Resistive AC-coupled Silicon Detectors (RSD, or AC-LGAD).

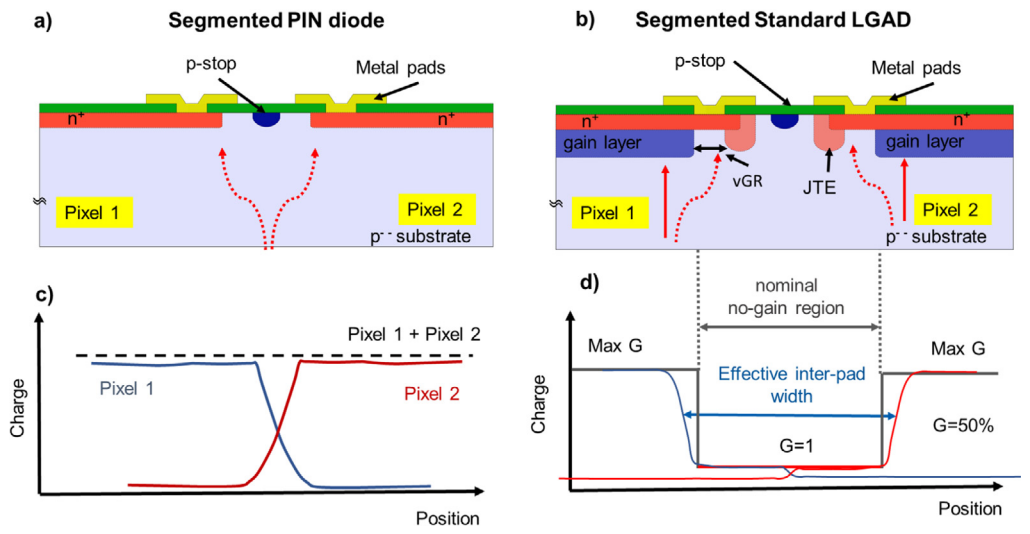

Fig. 1. Schematic drawings of a segmented PIN diode (a) and of a segmented LGAD (b). A sketch of the generated signals from PIN and LGAD are reported in (c) and (d), respectively.

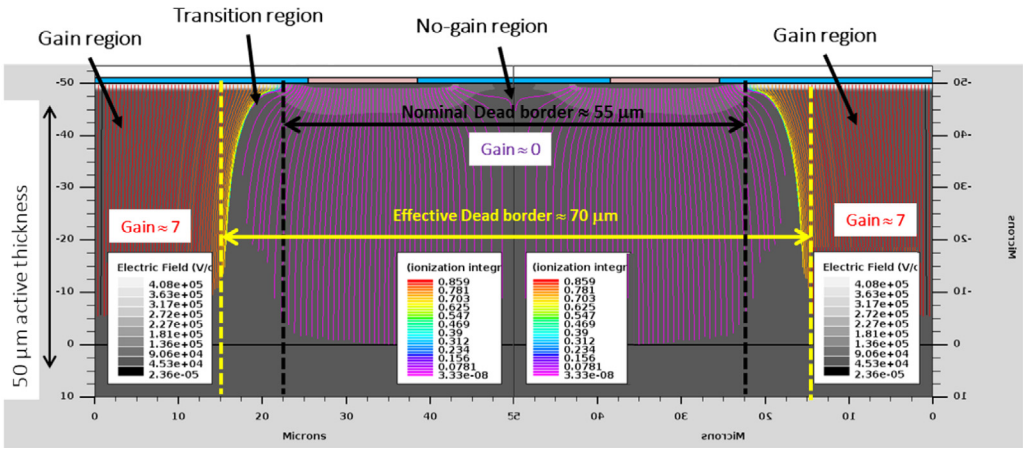

Fig. 2. TCAD Simulation of LGAD sensor. The electric field intensity at the border region between two pixel is represented by the gray-scale map. Solid lines show the carriers path through the junction, while the lines color represents the ionization integral value. (For interpretation of the references to color in this figure legend, the reader is referred to the web version of this article.)

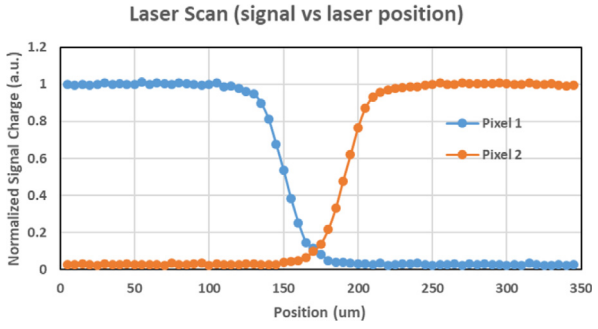

Fig. 3. Signal charge vs position of the laser, scanning the inter-pad region of a standard-LGAD with a nominal no-gain region of 31 µm.

The Standard LGAD segmentation has been described in the previous section. In Double-sided LGADs (or inverted-LGAD), the junction and the gain layer are not-segmented and the read-out segmentation is transferred on the back side of the sensor, where p^+ contacts are defined [2,16]. These sensors are typically produced on thick (about 300 µm) silicon wafers with a double-sided fabrication process. Using this integration scheme, it is possible to produce pixels with 100% FF and a uniform response along the sensitive region [17].

The third technology is the so-called Trench-Isolated LGAD (TI-LGAD). In this new design, the electrical isolation among pixels is obtained by means of trenches, physically etched in the silicon and filled with silicon oxide. Such an isolation scheme makes possible to reduce the no-gain width down to a few microns without affecting the detector performance.

The fourth scheme represents the Resistive AC-coupled Silicon Detectors (RSD or AC-LGAD), in which the multiplying junction is created using a resistive n^+-layer. In these sensors, the n^+-layer and gain layer are not segmented and the read-out segmentation is provided by metal pads that are AC-coupled to the resistive n^+-layer via a thin dielectric layer.

Both TI-LGADs and RSD technologies will be presented in the following parts of this section.

3.1. Trench-isolated LGAD

An alternative technological solution for the isolation of adjacent components in an integrated circuit device is the so-called Deep Trench Isolation (DTI) technique. This technology consists in the etching of

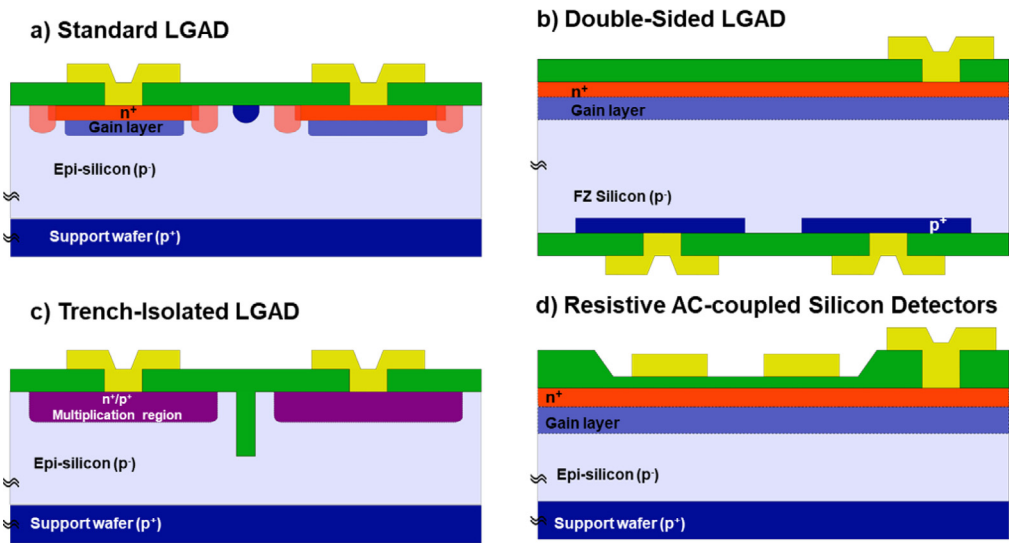

Fig. 4. Schematic drawings of different segmentation technologies for LGAD: (a) Standard segmentation; (b) Double-Sided LGAD; (c) Trench-Isolated LGAD; (d) Resistive AC-coupled Silicon Detectors.

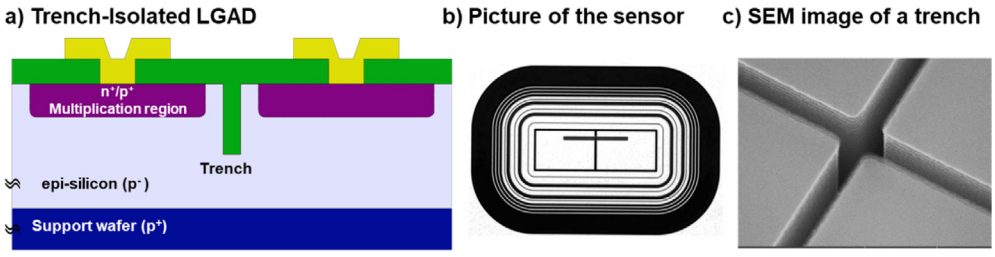

Fig. 5. (a) Schematic drawing of a TI-LGAD; (b) picture of a 1 × 2 array (the narrow rectangular aperture in the metal crossing the two pixels is used as entrance window during the laser scan; (c) SEM image of a trench before filling.

a pattern of trenches in the silicon substrate. The trenches are subsequently filled with dielectric materials, such as silicon dioxide.

In the past years, DTI has been extensively used for pixel isolation in CMOS image sensors [18], as well as in other avalanche detectors, such as Silicon Photomultipliers (SiPM) [19]. In particular, in SiPMs, DTI are also used as an optical barrier to reduce the internal optical cross-talk among adjacent pixels [20].

Trench-Isolated LGADs exploit DTI technology to provide electrical isolation among the pixels of a segmented LGAD. A schematic cross sectional view of TI-LGAD is reported in Fig. 5a. While the multiplying junction scheme (n^+-p^+-p^--p^+) remains the same as standard-LGADs, all the junction termination and isolation structures (JTE and p-stop) are here completely replaced by a single trench, that is less than 1 μm wide. This design offers a clear advantage in terms of reduction of the no-gain region between the pixels and overcomes the technological limitations of the standard technology described in the previous section.

The trench is etched in the silicon substrate during the fabrication process by means of the Deep Reactive Ion Etching (DRIE) technique, which is able to produce submicron trenches with high aspect ratio (up to 20 : 1). A Scanning Electron Microscope (SEM) image of a trench after the etching process is shown in Fig. 5c. After the etching, the trenches are filled with silicon dioxide to passivate the trench surface and to recover the wafer planarity. The first production of TI-LGAD has been carried out at FBK in 2019. A detailed description of the first prototypes and of their characterization can be found in [15].

Preliminary TCAD simulations of these devices show that DTI is effective in reducing the no-gain width down to 4 μm, a factor of five narrower than in state-of-the-art standard LGADs, without affecting the detector performance. The resulting simulated inter-pad width is thus reduced down to 5.5 ± 0.5 μm, as discussed in [15].

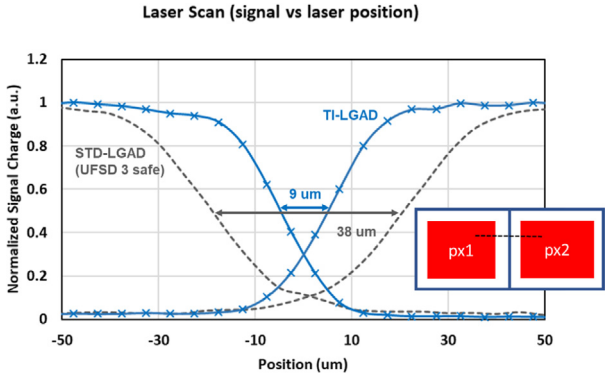

Fig. 6. Laser scan through the inter-pad region (represented in the inset) of a TI-LGAD (blue solid line with crosses) and of a standard-LGAD (dark gray dotted line).

The first produced samples have been characterized by means of a TCT setup and a IR laser source (as described in the previous section). Fig. 6 reports in blue the signals from two adjacent pads of the sensor in Fig. 5b (a 1 × 2 pads array, with pad size equal to 275 μm × 375 μm). The laser has been swept along an optical window (an aperture in the metal that crosses the two pixels) shown in Fig. 5b. The same measurement, carried out on a standard-LGAD with a 31 μm wide no-gain region, is plotted for reference. Both the sensor are biased at 200 – 250 V in order to set the same gain for both the devices (G = 15).

The measured effective inter-pad width of the TI-LGAD sample is 9.0 ± 2.5 μm, much narrower with respect to that of the standard-LGAD

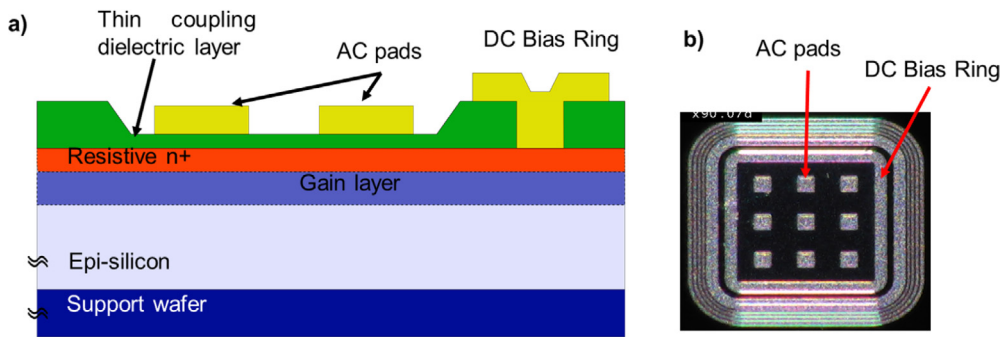

Fig. 7. Schematic drawing of Resistive Silicon Detectors (a); Picture of a 3 × 3 pads array produced at FBK (b).

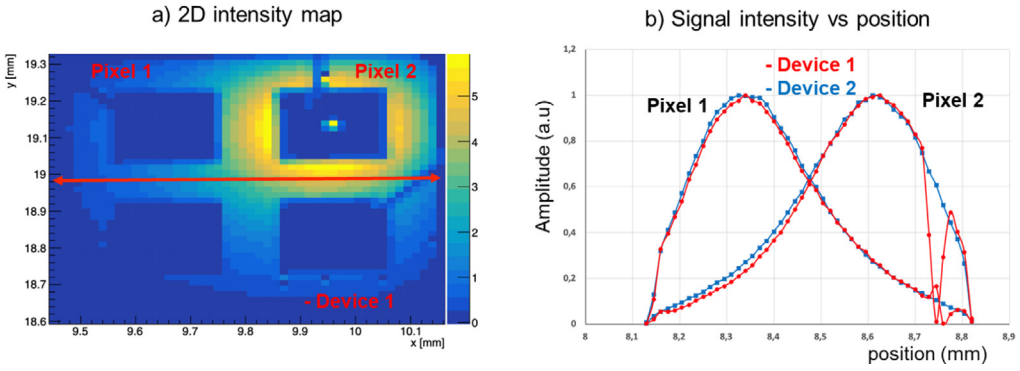

Fig. 8. Intensity map of the induced charge on pixel 2, obtained with a TCT setup (a). The sensor is a 2 × 2 pads array with 300 μm pitch. In (b) the signal from two adjacent pixels acquired with a laser scan along the red line in (a) is reported. Red and blue lines indicate two independent measurements on two identical devices. The red line corresponds to the device in (a) and the big fluctuation on the right is due to the presence of a bonding wire. (For interpretation of the references to color in this figure legend, the reader is referred to the web version of this article.)

(38.0 ± 2.5 μm). In addition, since the two channels are acquired simultaneously, it is possible to demonstrates that good electrical isolation between the pads is provided by the DTI technology. It should be noted that the measured inter-pad width of TI-LGAD is slightly larger than the simulated one (a discrepancy of 3.5 μm). Further investigations are still ongoing to explain this difference.

With the TI-LGAD technology it would be possible to produce segmented sensors with square pixels of 100 μm or 50 μm pitches with a remarkable FF of 83% and 67%, respectively. This estimation is done by considering the experimental value of the inter-pad width (9 μm).

3.2. Resistive AC-coupled silicon detectors

A schematic cross section of an RSD sensor is reported in Fig. 7a, together with a picture of a 3 × 3 pad array produced at FBK (in Fig. 7b). This sensor is designed following the principle of AC-coupled LGADs [21,22], and optimized for 4D tracking applications. The first production of these sensors has been carried out in the framework of the RSD project, and presented in [23,24].

In RSD, the n^+ electrode and the gain layer extend along the entire sensor area, without any patterning, thus providing a uniform gain through the sensor. The sensor segmentation is achieved via AC-coupled metal pads that lie on a thin dielectric film, while at the sensor periphery, the n^+ electrode is connected to the ground via an ohmic contact. The size of the AC metal pads determines the readout segmentation, while the thickness of the dielectric layer determine the capacitive coupling between the pads and the n^+ layer. The sensors have been fabricated on silicon wafers with a 50 μm thick epitaxial layer by means of a single-sided fabrication process, based on that used for the production of standard-LGAD, and described in [7]. The major differences with respect to the standard fabrication process regards the tuning of the n^+ sheet resistance and the local thinning of the top dielectric layer, aimed at finely selecting the capacitive coupling between pads and the n^+ electrode.

The signal formation process in RSD is substantially different from that of a standard LGAD, as explained in [25]: in RSD, the signal at the readout pads is mainly induced after that the charge carriers are collected at the front junction and they propagate laterally along the n^+ layer, discharging to the ground. This mechanism is the equivalent of the propagation of a signal in a lossy transmission line. The main advantage of this readout scheme is that the signal is shared among multiple pads, hundreds of microns far from the hit point. The signal sharing through the resistive layer enhances the spatial resolution of the sensor beyond the one achievable with segmented DC sensors (typically quoted as pixel size/$\sqrt{12}$), even at normal particle incidence.

Fig. 8a reports a laser scan of the detector surface carried out with the same TCT setup mentioned in Section 2. Each point of the image represents the intensity of the signal generated on a single pad of a 2 × 2 pixels sensor with 300 μm pitch. It is worth noting that the signal intensity decreases radially with the distance from the pad. This can be observed even better in Fig. 8b, where the signal sharing between two neighboring pixels is measured by means of a laser, scanning the sensor along the red line in Fig. 8a. It is important to stress that the sum of the signals from the two pixels is almost a constant along the inter-pad region, an evidence that RSD acts as a 100% FF sensor.

To fully exploit the spatial resolution capabilities of this sensor, the position of an hitting particles has to be calculated using a reconstruction algorithm that exploits the signals in multiple pixels. A simple estimation of the hits' coordinates can be done by using the amplitude-weighted centroid of the coordinates of four neighboring pads. Preliminary results about the RSD spatial resolution are presented in [26], where a resolution of 20 μm and 6 μm has been reported for sensors with 200 μm and 100 μm pitch, respectively. The extremely good spatial resolution, obtained with a relatively coarse segmentation, leads to important advantages in terms of number of required readout channels.

4. Conclusions

Latest developments of low gain avalanche detectors led this technology to a remarkable level of technological maturity, especially in particle tracking and timing applications. However, the spatial resolution of these sensors is still limited by their coarse segmentation, due to the presence of a no-gain region between adjacent pixels of about 50 μm. It has been demonstrated, also by means of TCAD simulations, as the standard segmentation approach of LGAD suffers from both intrinsic and technological limitations.

Several new segmentation strategies are currently being investigated to overcome these limitations. In particular, two new technologies have been discussed: TI-LGAD and RSD. The first one is able to reduce the inter-pad width down to 9 μm, enabling the possibility to design segmented sensors with fine pitch down to 50 μm. In the RSD technology instead, the improvement in the spatial resolution is reached by exploiting a completely different approach in the signal formation and read-out, which is based on AC-coupled electrodes. This readout mechanism enables charge sharing among the pixels, thus reaching a spatial resolution of 6 μm with a 100 μm pitch sensor.

Even if both these new technologies could be considered still at the first stage of development, they already showed very promising results that will be probably further enhanced in the next months thanks to improvements in the fabrication technology and in the sensor design.

Declaration of competing interest

The authors declare that they have no known competing financial interests or personal relationships that could have appeared to influence the work reported in this paper.

Acknowledgments

We thank our collaborators within RD50, ATLAS and CMS who participated in the development of UFSD. Part of this work has been financed by the European Union Horizon 2020 Research and Innovation funding program, under Grant Agreement no. 669529 (ERC UFSD669529), by the Italian Ministero degli Affari Esteri, by INFN Gruppo V, Italy and by the Dipartimento di Eccellenza, University of Torino, Italy (ex L. 232/2016, art. 1, cc. 314, 337). Some of the sensor productions presented in this work have been co-financed by FBK in the framework of the FBK-INFN agreement.

References

[1] G. Pellegrini, P. Fernández-Martínez, M. Baselga, C. Fleta, D. Flores, V. Greco, S. Hidalgo, I. Mandić, G. Kramberger, D. Quirion, M. Ullan, Technology developments and first measurements of low gain avalanche detectors (lgad) for high energy physics applications, Nucl. Instrum. Methods Phys. Res. A 765 (2014) 12–16, http://dx.doi.org/10.1016/j.nima.2014.06.008.

[2] G. Pellegrini, M. Baselga, M. Carulla, V. Fadeyev, P. Fernández-Martínez, M.F. García, D. Flores, Z. Galloway, C. Gallrapp, S. Hidalgo, Z. Liang, A. Merlos, M. Moll, D. Quirion, H. Sadrozinski, M. Stricker, I. Vila, Recent technological developments on lgad and ilgad detectors for tracking and timing applications, Nucl. Instrum. Methods Phys. Res. A 831 (2016) 24–28, http://dx.doi.org/10.1016/j.nima.2016.05.066.

[3] H.F.-W. Sadrozinski, A. Seiden, N. Cartiglia, 4d tracking with ultra-fast silicon detectors, Rep. Progr. Phys. 81 (2) (2017) 026101, http://dx.doi.org/10.1088/1361-6633/aa94d3.

[4] N. Cartiglia, R. Arcidiacono, B. Baldassarri, M. Boscardin, F. Cenna, G. Dellacasa, G.-F.D. Betta, M. Ferrero, V. Fadeyev, Z. Galloway, S. Garbolino, H. Grabas, V. Monaco, M. Obertino, L. Pancheri, G. Paternoster, A. Rivetti, M. Rolo, R. Sacchi, H. Sadrozinski, A. Seiden, V. Sola, A. Solano, A. Staiano, F. Ravera, A. Zatserklyaniy, Tracking in 4 dimensions, Nucl. Instrum. Methods Phys. Res. A 845 (2017) 47–51, http://dx.doi.org/10.1016/j.nima.2016.05.078.

[5] M. Ferrero, R. Arcidiacono, M. Barozzi, M. Boscardin, N. Cartiglia, G. Dalla Betta, Z. Galloway, M. Mandurrino, S. Mazza, G. Paternoster, et al., Radiation resistant lgad design, Nucl. Instrum. Methods Phys. Res. A 919 (2019) 16–26.

[6] V. Sola, R. Arcidiacono, M. Boscardin, N. Cartiglia, G.-F.D. Betta, F. Ficorella, M. Ferrero, M. Mandurrino, L. Pancheri, G. Paternoster, A. Staiano, First fbk production of 50 μm ultra-fast silicon detectors, Nucl. Instrum. Methods Phys. Res. A 924 (2019) 360–368, http://dx.doi.org/10.1016/j.nima.2018.07.060.

[7] G. Paternoster, R. Arcidiacono, M. Boscardin, N. Cartiglia, F. Cenna, G.D. Betta, M. Ferrero, R. Mulargia, M. Obertino, L. Pancheri, C. Piemonte, V. Sola, Developments and first measurements of ultra-fast silicon detectors produced at FBK, J. Instrum. 12 (02) (2017) C02077, http://dx.doi.org/10.1088/1748-0221/12/02/c02077.

[8] M. Andrä, J. Zhang, A. Bergamaschi, R. Barten, C. Borca, G. Borghi, M. Boscardin, P. Busca, M. Brückner, N. Cartiglia, S. Chiriotti, G.-F. Dalla Betta, R. Dinapoli, P. Fajardo, M. Ferrero, F. Ficorella, E. Fröjdh, D. Greiffenberg, T. Huthwelker, C. Lopez-Cuenca, M. Meyer, D. Mezza, A. Mozzanica, L. Pancheri, G. Paternoster, S. Redford, M. Ruat, C. Ruder, B. Schmitt, X. Shi, V. Sola, D. Thattil, G. Tinti, S. Vetter, Development of low-energy X-ray detectors using LGAD sensors, J. Synchrotron Radiat. 26 (4) (2019) 1226–1237, http://dx.doi.org/10.1107/S1600577519005393.

[9] A. Vignati, V. Monaco, A. Attili, N. Cartiglia, M. Donetti, M.F. Mazinani, F. Fausti, M. Ferrero, S. Giordanengo, O.H. Ali, et al., Innovative thin silicon detectors for monitoring of therapeutic proton beams: preliminary beam tests, J. Instrum. 12 (12) (2017) C12056.

[10] P. Fernández-Martínez, D. Flores, S. Hidalgo, V. Greco, A. Merlos, G. Pellegrini, D. Quirion, Design and fabrication of an optimum peripheral region for low gain avalanche detectors, Nucl. Instrum. Methods Phys. Res. A 821 (2016) 93–100, http://dx.doi.org/10.1016/j.nima.2016.03.049.

[11] V. Sola, R. Arcidiacono, M. Boscardin, G. Borghi, N. Cartiglia, M. Centis Vignali, M. Costa, G.F. Dalla Betta, M. Ferrero, M. Mandurrino, L. Pancheri, G. Paternoster, F. Ficorella, A. Staiano, F. Siviero, M. Tornago, Interpad optimisation strategies on lgad manufactured at fbk, in: 35th RD50 Workshop (CERN), CERN, 2019.

[12] F. Siviero, et al., Innovative tct studies on the breakdown of ufsd3 sensors by fbk, in: 33rd RD50 Workshop, CERN, Geneva, Switzerland, 2018, URL https://indico.cern.ch/event/754063/contributions/3222653/.

[13] M. Tornago, et al., Performances of the third ufsd production at fbk, in: Presented at 33rd RD50 Workshop, CERN, Geneva, Switzerland, 2018, URL https://indico.cern.ch/event/754063/contributions/3222642/.

[14] SILVACO ATLAS, User's Manual, https://dynamic.silvaco.com/dynamicweb/jsp/downloads/DownloadManualsAction.do?req=silentmanuals&nm=atlas.

[15] G. Paternoster, G. Borghi, M. Boscardin, N. Cartiglia, M. Ferrero, F. Ficorella, F. Siviero, A. Gola, P. Bellutti, Trench-isolated low gain avalanche diodes (ti-lgads), IEEE Electron Device Lett. 41 (6) (2020) 884–887.

[16] G.-F.D. Betta, L. Pancheri, M. Boscardin, G. Paternoster, C. Piemonte, N. Cartiglia, F. Cenna, M. Bruzzi, Design and tcad simulation of double-sided pixelated low gain avalanche detectors, Nucl. Instrum. Methods Phys. Res. A 796 (2015) 154–157, http://dx.doi.org/10.1016/j.nima.2015.03.039.

[17] E. Currás, M. Carulla, M.C. Vignali, J. Duarte-Campderros, M. Fernández, D. Flores, A. García, G. Gómez, J. González, S. Hidalgo, et al., Inverse low gain avalanche detectors (ilgads) for precise tracking and timing applications, Nucl. Instrum. Methods Phys. Res. A 958.

[18] T. Arnaud, F. Leverd, L. Favennec, C. Perrot, L. Pinzelli, M. Gatefait, N. Cherault, D. Jeanjean, J.-P. Carrere, F. Hirigoyen, L. Grant, F. Roy, Pixel-to-pixel isolation by deep trench technology: Application to cmos image sensor, 2011.

[19] C. Piemonte, F. Acerbi, A. Ferri, A. Gola, G. Paternoster, V. Regazzoni, G. Zappala, N. Zorzi, Performance of nuv-hd silicon photomultiplier technology, IEEE Trans. Electron Devices 63 (3) (2016) 1111–1116, http://dx.doi.org/10.1109/TED.2016.2516641.

[20] C. Dietzinger, P. Iskra, T. Ganka, T. Eggert, L. Höllt, A. Pahlke, N. Miyakawa, M. Fraczek, J. Knobloch, F. Wiest, W. Hansch, R. Fojt, Reduction of optical crosstalk in silicon photomultipliers, in: H. Mohseni, M.H. Agahi, M. Razeghi (Eds.), Biosensing and Nanomedicine V, Vol. 8460, International Society for Optics and Photonics, SPIE, 2012, pp. 223–231, http://dx.doi.org/10.1117/12.930473.

[21] N. Cartiglia, R. Arcidiacono, M. Baselga, R. Bellan, M. Boscardin, F. Cenna, G.D. Betta, P. Fernndez-Martnez, M. Ferrero, D. Flores, Z. Galloway, V. Greco, S. Hidalgo, F. Marchetto, V. Monaco, M. Obertino, L. Pancheri, G. Paternoster, A. Picerno, G. Pellegrini, D. Quirion, F. Ravera, R. Sacchi, H.-W. Sadrozinski, A. Seiden, A. Solano, N. Spencer, Design optimization of ultra-fast silicon detectors, Nucl. Instrum. Methods Phys. Res. A 796 (2015) 141–148, http://dx.doi.org/10.1016/j.nima.2015.04.025.

[22] G. Giacomini, W. Chen, G. D'Amen, A. Tricoli, Fabrication and performance of ac-coupled lgads, J. Instrum. 14 (09) (2019) P09004.

[23] M. Mandurrino, R. Arcidiacono, M. Boscardin, N. Cartiglia, G.F. Dalla Betta, M. Ferrero, F. Ficorella, L. Pancheri, G. Paternoster, F. Siviero, M. Tornago, Demonstration of 200-, 100-, and 50- μ m pitch resistive ac-coupled silicon detectors (rsd) with 100 4d particle tracking, IEEE Electron Device Lett. 40 (11) (2019) 1780–1783, http://dx.doi.org/10.1109/LED.2019.2943242.

[24] M. Mandurrino, R. Arcidiacono, M. Boscardin, N. Cartiglia, G.-F. Dalla Betta, M. Ferrero, F. Ficorella, L. Pancheri, G. Paternoster, F. Siviero, et al., Analysis and numerical design of resistive ac-coupled silicon detectors (rsd) for 4d particle tracking, Nucl. Instrum. Methods Phys. Res. A 959 (2020) 163479.

[25] N. Cartiglia, R. Arcidiacono, G. Borghi, M. Boscardin, M. Costa, Z. Galloway, F. Fausti, M. Ferrero, F. Ficorella, M. Mandurrino, S. Mazza, E. Olave, G. Paternoster, F. Siviero, H.F.-W. Sadrozinski, V. Sola, A. Staiano, A. Seiden, M. Tornago, Y. Zhao, LGAD Designs for Future Particle Trackers, Vol. 979, 2020, p. 164383, http://dx.doi.org/10.1016/j.nima.2020.164383, URL http://www.sciencedirect.com/science/article/pii/S0168900220307804.

[26] R. Arcidiacono, G. Borghi, M. Boscardin, N. Cartiglia, M. Costa, G.D. Betta, F. Fausti, M. Ferrero, F. Ficorella, M. Mandurrino, S. Mazza, E. Olave, L. Pancheri, G. Paternoster, H.-F. Sadrozinski, V. Sola, A. Staiano, A. Seiden, F. Siviero, M. Tornago, Y. Zhao, State-of-the-art and Evolution of UFSD Sensors Design at FBK, Vol. 978, 2020, p. 164375, http://dx.doi.org/10.1016/j.nima.2020.164375, URL http://www.sciencedirect.com/science/article/pii/S0168900220307725.